ASPECTS OF TEMPORAL AND SPATIAL RANGING FOR BISTATIC SUBMARINE LIDAR

Uwe Stute[1], Michel Lehaitre[1] and Olga Lado-Bordowsky[2]

1. TMSI/ME Ifremer, BP 70, F-29280 Plouzané, France. Email: uwstute@compuserve.de
2. ENSSAT , BP 447, F-22405 Lannion CEDEX

ABSTRACT

For a long time underwater optics has provided interesting information in oceanography, and bio-optics has become an important tool for biologists in marine ecology studies. But the difficulties caused by a turbid medium and the dynamics of currents led to the necessary development of new techniques. In this context a versatile Underwater LIDAR Imaging System (ULIS) has been developed to improve underwater imaging and to study tomoscopic aspects of laser-induced elastic and inelastic backscattering.

The presented studies are focused on the bistatic design of LIDAR combined with a spectral analysis of the backscattered signal for tomoscopic application. The data were obtained with a frequency doubled Nd:YAG (λ=532 nm) and a gated angular resolved detection. While the time base of the system can be compared to ranging of other on-axis LIDAR (2,6,11), the spatial dimension of the signal brings complementary information by the light flux distribution as a function of the angle of incidence. The analysis of the bistatic angular resolved detection is focussed on two axes: one target of investigation is the impact of scattering during the light propagation and the second axis investigates temporal aspects of fluorescence in near field data of this LIDAR. Both targets of investigation, scattering and temporal aspects of fluorescence, have a significant impact on LIDAR measurements and can *in-situ* only be investigated with a detection using simultaneously spatial and temporal ranging facilities, like it can be done with ULIS.

First sea trials with this LIDAR have shown the potential for the investigation of fluorescence profiles even in very turbid estuaries. A large area could be covered, once the system is integrated in a towed platform. This initial option could be realized with minor changes, as the concept of the platform has already taken into account operational aspects.

THE LIDAR SYSTEM

The system contains five watertight housings, three of them are carrying the laser, the camera with the mounted spectrometer and the passive collector *optenne* as the optical parts. The modem for the data transfer and the micro PC for the system management are the last two logistical parts.

The innovative feature of this system is its bistatic design with an angular resolved detection. The system is installed in a frame and the distance between the laser and the optical receiver may vary from 0.17 m to about 1.70 m. In Figure 1 the system is drawn illustrating two of the 12 detection channels. These channels each have a mean angle of detection in the plane defined by the laser beam and the optical axis of the collector. The detection channel j is illustrated with its mean angle a_j in respect to the optical axis of the receiver. For light hitting the detector, the angle of incidence a is related to the scattering angle y by $y = 180° - a$; therefore the detection channel which detects the signal from the time gated volume varies with the distance. The in water angular range of the receiver goes from 8° to -2°. The maximal aperture of the detection unit leads to an uncovered near-field defined by the distance between the collector and the laser axis . The disadvantage of a shadowed area in the near field was accepted to permit an angular discrimi-

nation of returned light. The signal of each detection channel provides an entire spectrum, hence, spectral analysis can be achieved in respect of the angle of incidence.

Gated angular resolved detection with spectral discrimination

To permit geometric discrimination of a gated signal, a set of angular channels must be simultaneously detected. Following experiments conducted by IFREMER, a spectrometer separating the signal of 50 fibres was chosen.

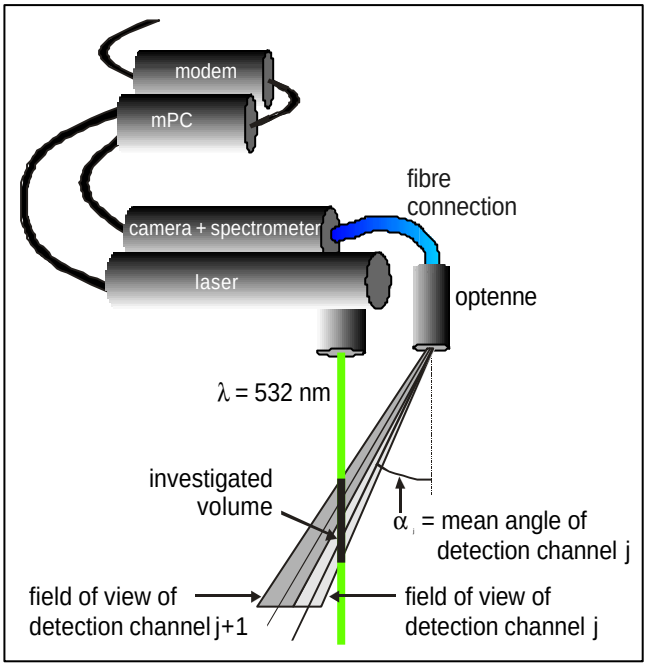

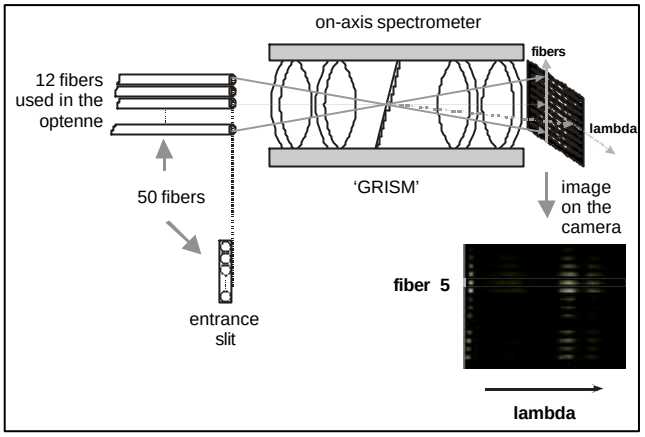

Figure 1 (above): Schema of the on-axis spectrometer

Figure 2 (left): Schema of the bistatic LIDAR

The detection is composed of two separated containers connected by a fibre bundle, one being the totally passive collector *optenne*, [1] which couples light according to the angle of incidence into a set of 12 fibres. Each fibre represents, on the other hand, the entrance slit of the on-axis transmission spectrometer. The particularity of this spectrometer is its on-axis concept, which has the advantage for marine applications, that the detection can be integrated in tubes with standard diameters. The spectrometer is mounted on the IR-enhanced time-gated camera to image the matrix [fibres x λ] on the CCD array as illustrated in Figure 2.

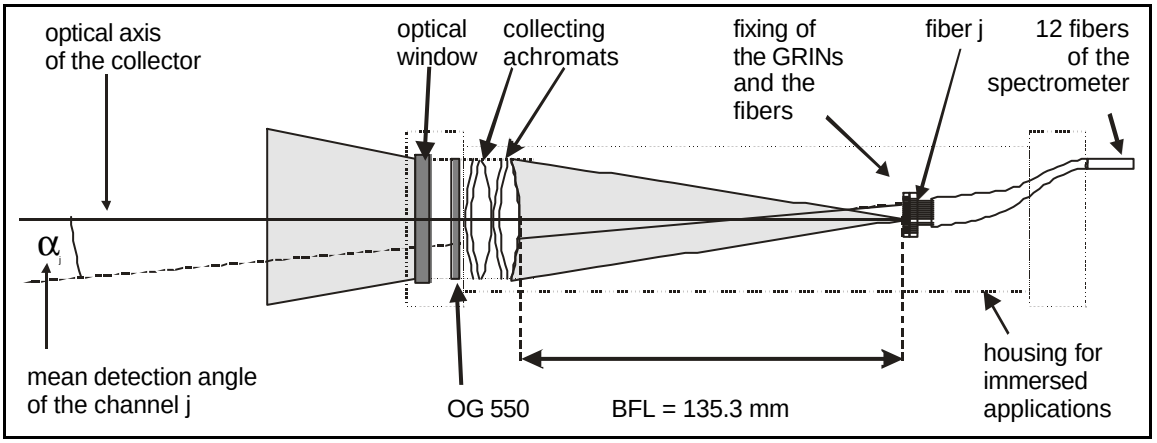

Figure 3: Schema of the optenne with its angular resolved detection

[1] The name optenne stands for "optical antenna" to describe the total passive collection of light injected into fibres for further photometric analysis, which couples light according to the angle of incidence into a set fibres.

The *optenne* used in this study focuses the incident light with a set of two achromatic doublets. In the back-focal-plane 12 gradient index lenses coupled the light into the corresponding fibres. Due to its very high backscattering efficiency compared to the fluorescence, the elastic scattering is attenuated with an orange glass filter (OG 550) in front of the achromatic lenses to obtain an elastic scattering signal of the same order of magnitude as the fluorescence signals.

Table 1: Most relevant technical data

Laser	Type	Nd YAG 3+
Brilliant	Energy per pulse	110 mJ @ 532 nm
by Quantel S.A.	Pulse length	6 ns
	Repetition rate	25 Hz
Detector	Diameter	82 mm
	Back focal length	79 mm
Spectrometer	Resolution	2 nm
prototype from Instruments S.A. Div. Jobin Yvon	Fibres used / total	14 / 54
Camera	Type	Standard CCIR
IP 800 CC 11	Pixel	754 x 580
from Philips S.A.S	Opening	5 ns-19.3 ms
	Frame rate	50 Hz non interlaced
Time base	Minimal step	1.2 ns

On the CCD array the signal of a detection channel corresponds to 11 pixels lines for fibres in the centre of the entrance slit and to 12 lines for off-axis fibres. Each line represents a spectra from 400 nm to 750 nm. In order to compare the received signal of different detection channels, the sensitivity function of each fibre has been determined.

For the evaluation of the platform, the small size of the receiving unit was useful, as it is easy to handle and allows to study in a simple way the optimum distance between the laser and the *optenne* axis. We consider the potentiality for using a set of (different) *optennes* based on the same spectral analysis to be important, as this facility permits a great variety of configurations for the whole system e.g. to perform angular discrimination in the far field by using a set of such detectors. The most relevant data of the system are given in Table 1.

Time base

The ranging by the system is based on the delay between the laser pulse (with a duration of about 6 ns) and the gated camera with a minimum aperture of about 7 ns. The delay is generated by the micro PC in minimal steps of 1.2 ns with a maximum of 300.9 ns. Taking into account the light velocity in water, we have a maximum distance resolution of 0.13 m for the centre of the investigated volume and a width of 1.35 m.

The system control allows the programming of series of up to 100 delays in the sequence mode. Between each step, the power of the laser may be adapted to the attenuation of the water column. This is achieved by a delay between the maximal intensity of the pumping flash lamps and the Q-switch. The laser power can be reduced to 20 % of the maximal value. The time to get an acceptable profile depends on the turbidity and the maximal distance (15). The signal to noise ratio determines the number of images to be averaged

at a spatial point, therefore acquisition time of a profile increases exponentially with distance and with turbidity.

BISTATIC ASPECTS OF MARINE LIDAR

The signal analysis is focused on two axes to process the information from the angular resolved bistatic LIDAR. First, the relation between scattering and changes in the angular signal distribution is investigated; the radial distribution of the laser induced irradiance is on the one hand determined by scattering and on the other by its impact on the geometric interpretation of the signal. Secondly, the geometry is used as a ranging facility (14) to survey temporal scale; for an investigated volume with a known radial extent, changes in the spatio-temporal signal can be associated with the temporal scale of the optical process like the observed fluorescence life time ? ? F.

To illustrate the capacity of the system to analyse particle scattering and temporal aspects of fluorescence, the signal evolution during an algae bloom in a tank trial is presented. The algae have been growing for five days in an open tank, illuminated by intense summer sunlight. Biologists from IFREMER have determined the species with a microscope and found a typical coastal summer population of diatoms[2], some flagellates and a small amount of detritus. Water samples on this day had a mean chlorophyll-a content of 0.72 +/- 0.03 mg/m3 and a mean phaeopigment concentration of 0.40 +/- 0.08 mg/m3.

The measured signals lead to interesting observations for scattering and fluorescence. The theory to extract the corresponding forward scattering coefficient bf and ? ? F is, for the sake of the volume of the article, not integrated and only the sketch of the interpretation and tendencies found in the data are reported.

The spatio-temporal signal of ULIS

The main difference between the monostatic and the bistatic LIDAR signal is due to the shape of the investigated volume. LIDARs with gated detection limit the investigated volume on the ranging axis by their time base. The signal represents the integration of the amplitude of the gated convolution of the laser pulse S(R). In ULIS the signal of each detection channel j is furthermore determined by its field of view FOVj. A schema for the geometrical and the temporal limits of the investigated volume is illustrated in Figure 4.

Each detection channel has a different mean detection angle with regard to the optical axis of the collector in the range of –1.6° to 5.6° in water and a divergence of 0.9°. At the distance R, the signal distribution over the detection channels is related to the individual overlap factors Aj (10) between the FOVj of each channel j and the radial irradiance distribution.

The first signal analysis approach uses immediate optical processes, which means that the amplitude function S(R) can be computed from the gated convolution of laser pulse shape over the detection time ? D. The signal is then an implicit function of the radial distribution of the laser induced irradiance, which determines the geometric overlap of each detection channel. The second approach uses the determined radial irradiance distribution up to the range R to compute the amplitude function S(R). A variation of S(R) must be attributed to optical processes having a time scale in the same order as the ranging time base of the LIDAR.

Both methods provide stable signals for variations of the temporal parameters (laser pulse shape, gated detection), while the signal is sensitive to a variation of the detection geometry; the correlation decreases by less than 2% with variations of the temporal parameters up to 15%. The calibration of the FOV_j of the detection was, therefore, of major importance.

[2] The major species are the diatoms *Chaeotoceros perpusillum, Chaeotoceros didymus, Chaeotoceros curvisetum, Rhizosolenia delicatula, Skeletonema costatum*

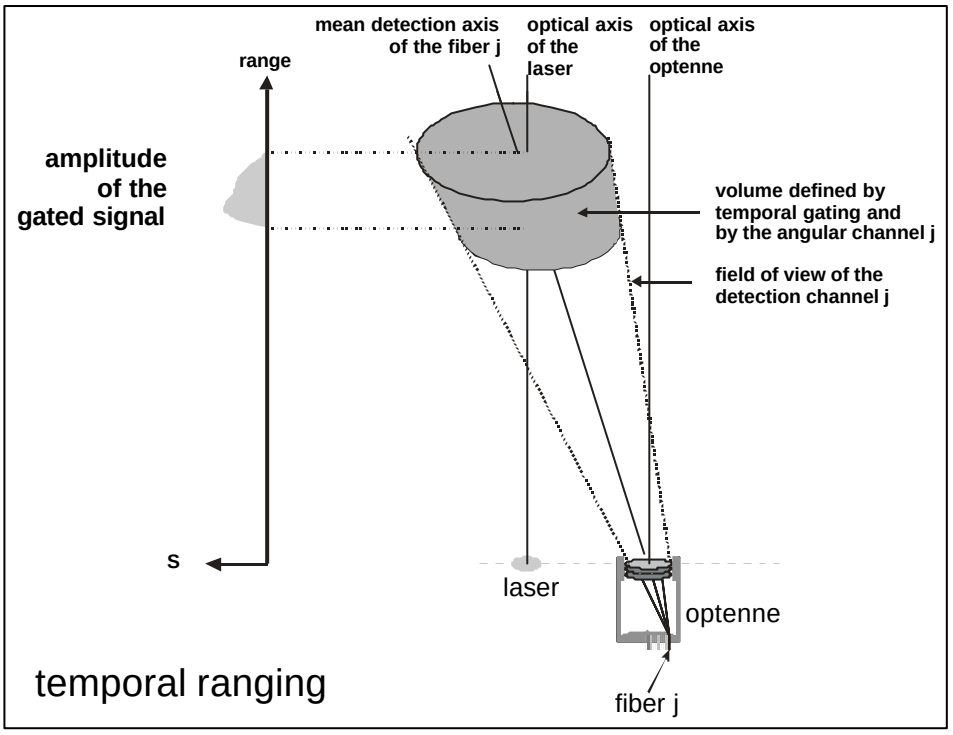

Figure 4: **Illustration of the volume defined by temporal ranging and the field of view of a detection channel with ULIS. The temporal ranging determines the signal as a function of the distance, while the angular channels determines the perpendicular extend.**

Temporal ranging facility: Scattering

To understand the analysis of scattering, the signal has to be separated into the spatial and the temporal aspects. The detected Raman signal at *R* is composed of the amplitude *S(R)* of the laser induced irradiance on the ranging axis, the distribution *D(R,r)* of the laser induced irradiance over the radial parameter r and constant factors like the Raman efficiency and the laser power. The significant impact of scattering on the angular distribution of the signal can be seen in the measurement illustrated in Figure 5, where the maximum normalised Raman signal for four programmed delays is illustrated in a water mass containing an algae population with a high density. The attenuation coefficient of c (λ = 660 nm) = 1.54 m^{-1} was determined by a transmissometer.

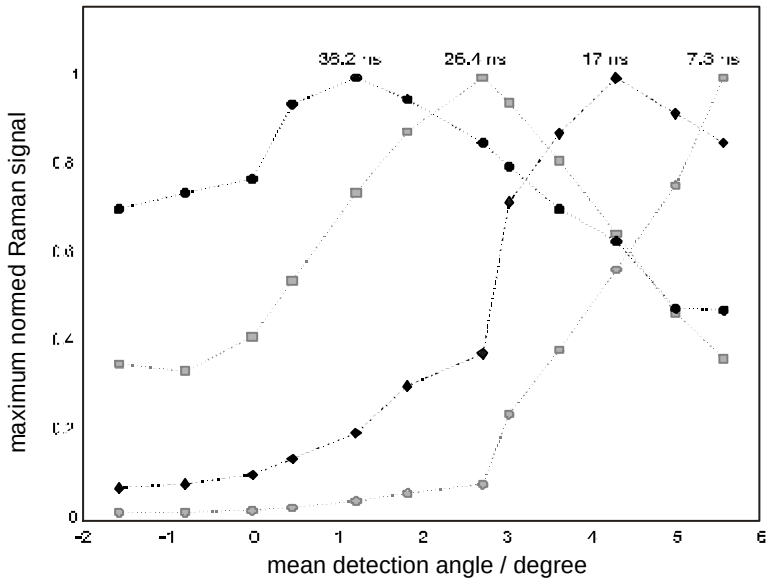

Figure 5: The angular resolved signal of a seawater mass with high content of marine phytoplankton. The response is illustrated for four programmed delays. The attenuation coefficient was *c*(660 nm) = 1.54 m^{-1}.

From the computation of theoretical signals it can be concluded that the shift of the maximum is induced by the control of the time base, while the variation of the shape is associated with changes in the radial irradiance distribution.

While the maximum corresponds to unscattered radiation, significant scattering appears in the signal with a wider angular distribution. In the maximum normalised measured signals, an offset in the angular range of the detection channels becomes visible and increases with the optical density of the water. In the measured data, a similar behaviour is observed for a fixed distance; the magnitudes of the offsets are related to the attenuation coefficients of different water masses. Without going into details, further processing was used to extract values for the mean forward scattering coefficient and provided stable values in the range of 4 to 7 m.

In conclusion, the LIDAR signal composed of spatial and temporal ranging elements can directly investigate forward scattering. The forward scattering coefficient b_f is an interesting parameter for turbidity studies in coastal waters.

Geometric ranging facility: Fluorescence

The temporal aspects of the laser stimulated optical processes depend on the properties of the seawater constituent A common method to identify compounds of the marine environment is spectral analysis; the Raman normalised spectra are given for four days of the trial in Figure 6. To have a rough classification of the emitting source, the signal is analysed for different spectral regions, attributed to Raman scattering for 638 nm < λ_R < 662 nm, to chlorophyll-a for 670 nm < λ_{em} < 690 nm and to various organic matter[3] for 550 nm <λ_{em} < 630 nm.

To analyse the temporal aspects of fluorescence, the composite signal must again be separated. As the ranging is based on the time lapse, the fluorescence life time must be integrated into the ranging on the propagation axis (10). Any delay in fluorescence emission leads to an offset, which has to be subtracted from the total amount of time elapsed between the laser emission and the detection. This means that the fluorescence amplitude function $S_F(R)$ can be found by the convolution of the system amplitude function $S(R)$ with the fluorescence decay.

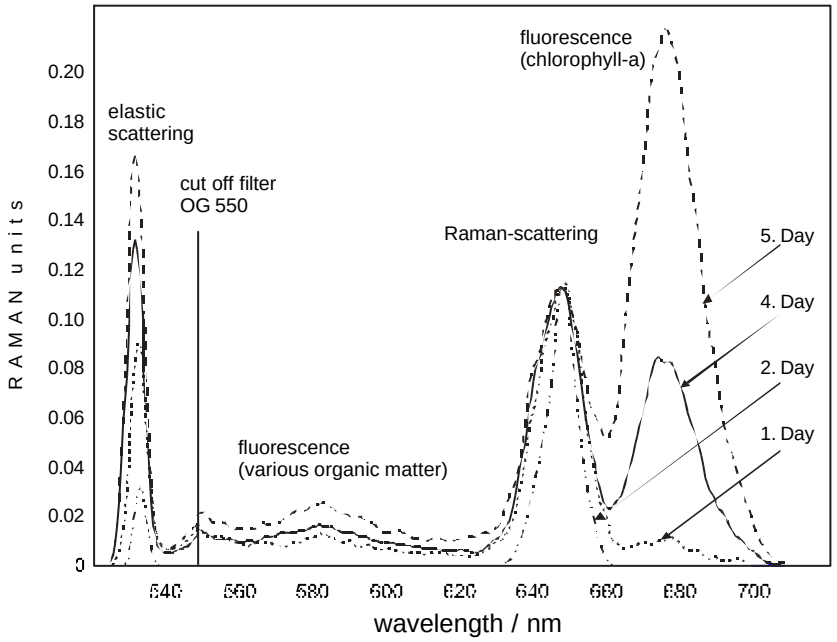

Figure 6: The measured spectra for days of the tank trial with the attribution of components. It is important to notice, that the elastic scattering is attenuated and therefore the values for wavelength smaller than 570 nm are only normalised relative to the Raman signal.

The gated signal acquires at the same time, the spectral response of all detection channels with the same geometrical parameters. This means that neither the geometry of ULIS nor the data acquisition are

[3] This wavelength region is attributed to CDOM, as the fluorescence efficiency in this wavelength region is low compared to the efficiency of the chlorophyll-a and, furthermore, billiproteins are not reported in the algae classes found in the water analysis.

changed; so, any influence from the data acquisition can be denied for gated signals and only their spectral domain is distinguished.

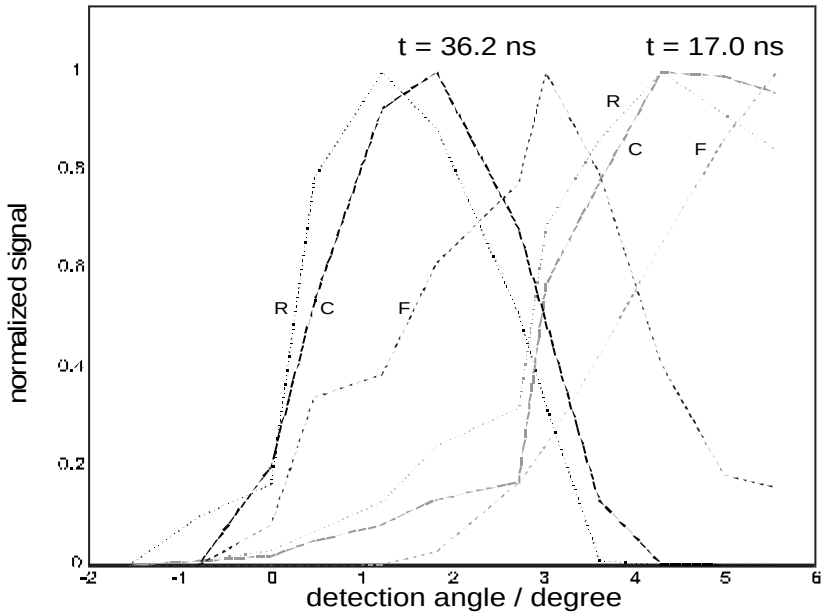

Figure 7 : Angular resolved representation of the signal of two gating times. The scattering offset was reduced by the signal at –1.7°. The graph show the intensity in fixed wavelength bands corresponding to water Raman scattering (638 nm<λ_R<662 nm) (line R), Chlorophyll-a fluorescence (670 nm<λ_{em}<690 nm) (line C), CDOM fluorescence (550 nm<λ_{em}<630 nm) (line F).

The angular distribution of the gated signal of different wavelength regions are presented in Figure 7 for two programmed delays. On a nanosecond scale Raman scattering is considered to be an instantaneous process, we can therefore assume that the maximum of the Raman signal marks the propagation of the laser pulse. Here, for both gating times, the CDOM fluorescence signal is more strongly shifted on the angular scale than the chlorophyll-a signal. This differences in the angular distribution of the wavelength bands must be attributed entirely to the temporal response of the emission.

The spatial ranging leads to a decrease of the incidence angle with increasing distance. Delayed emission is thus detected with greater angles of incidence. The maximum signal response of CDOM is, hence, more delayed than the response of the chlorophyll-a. This temporal shift can be attributed to a delay of the fluorescence emission in the order of some nanoseconds.

The response of an exponential fluorescence decay depending on the fluorescence life time in interaction with the laser beam attenuation has been studied. In the data the fluorescence response has defined maxima. For these maxima it has been found in theoretical computations, that they can only by displaced significantly by the interaction of the fluorescence delay with an attenuation coefficient c satisfying the necessary condition: $1/t_F > cn$ with propagation velocity n.

The consequences of signal processing are illustrated in Figure 8. Here a tomoscopic series of spectra achieved with the LIDAR is shown. This series is processed similarly as a telescopic on-axis LIDAR. This means, no angular resolved detection and the only ranging possibility for the incoming spectra is the temporal gating ability. Each spectrum was obtained by averaging 50 to 300 images. It can be noticed that each image provides the whole spectrum.

These spectra were obtained for a homogeneous water body[4] and are only distinguished by the delay between the laser pulse and the opening of the camera. For the sake of the presentation these spectra are normed to the maximum of Raman scattering, without taking into account the fluorescence base line and for the spectral sensitivity of detection. For a qualitative discussion, the effect of the fluorescence baseline has been estimated to be small (<5%).

[4] Stratification aspects seem not to be important, as the data sets for dense algae populations provide the same results on different days.

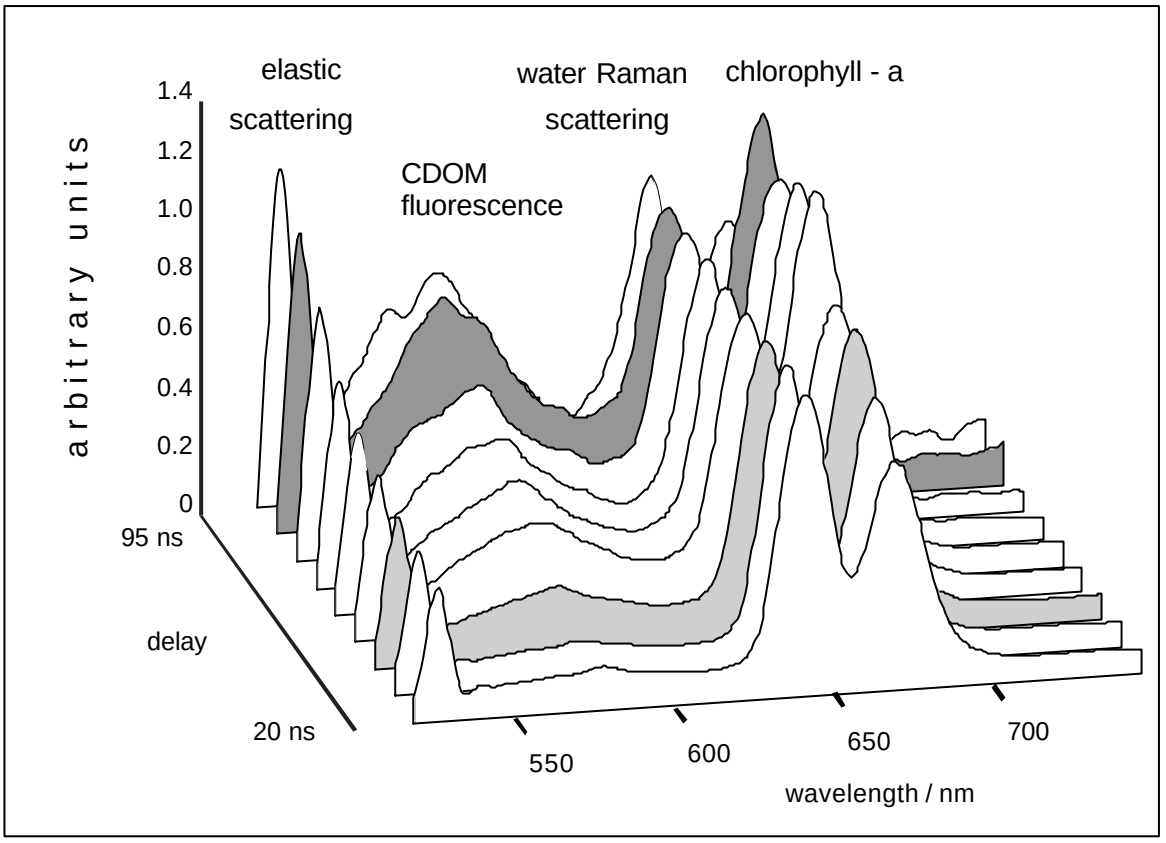

Figure 8: A series of spectra from the tank experiment, taken as a function of the programmed delay.

Since the water body is statistically homogeneous, the same response to excitation would be expected at any delay, but a relative variation of the signal over the spectral regions is observed.

While the elastic scattering is anisotropic, fluorescence of a bulk algae population is considered to be isotropic and hence independent of the detection geometry. The increase in elastic scattering (λ_{max}=532 nm) might be attributed to particle reflection, which is more important in smaller angles. The shape of the chlorophyll-a fluorescence (λ_{max} ~ 685 nm) has a rise, a stable phase and a decrease, while the CDOM increases with the delay.

In an attempt to explain this behaviour by the observed fluorescence lifetime, the quenching of excited molecules must be investigated. While DOM is composed of molecules, which are on the molecular scale far away from each other, the living cells have a compact structure and excitation transfer is reported by many authors (3,8). Excitation transfer means that the energy of an excited molecule corresponds to an absorption energy level of a close neighbour molecule (~10 nm), so the energy is transferred radiation free. In conclusion, the observed fluorescence life τ_F is related to the molecular fluorescence life time τ_M and depends on the neighbour molecules by radiation free transfer of excited states.

Based on the previous considerations found in the literature, we suggest phytoplanktonic energy transfer to be responsible for response of the chlorophyll-a. It can be supposed that with increasingly high photon density, the quenching rate by the environment of the chlorophyll-a decreases and the observed fluorescence life time increases. This corresponds to the analysis of the angular resolved signal, where the shift of the detection maximum decreases with the distance and vanishes, when the ratio between the Raman signal and the chlorophyll-a fluorescence becomes stable. With the work of Fadeev et al.1997 (5), the observed fluorescence efficiency can be explained for the irradiance levels, where fluorescence lifetime is not ob-

served. The apparent steady efficiency is supposed to be maintained by the absorption of the chlorophyll-a and by the radiation free transport of excitons from the accessory pigments. The radiation free energy transfer could buffer the emission level, as if only the direct reaction of the chlorophyll-a occurs, the maximum would be expected to be sharper. The decrease in the emission would represent the point where the photon density is less than the maximal transfer rate towards the chlorophyll-a.

The increase for CDOM fluorescence can be understood assuming a higher and constant fluorescence life time due to a lower and fixed quenching rate. The maximum in angular resolved detection was observed to be shifted by approximately constant values and suggests a constant quenching rate. It is probably not the fluorescence efficiency of CDOM which changes, but the temporal behaviour of the emission leads to apparent changes of the efficiency.

CONCLUSION

In conclusion, it can be stressed that there is a strong interaction between the time base of measurement and the optical properties of *in-vivo* phytoplankton and of CDOM. The additional ranging via geometric parameterisation consequently gives information from this interaction and seems to be useful in remote sensing. The observed changes in the angular detected signal have been used in further studies to extract the forward scattering coefficient and the fluorescence life time from LIDAR data. In this context, LIDAR seems to be sensitive to *in-vivo* phenomena, as the time scale for these processes is in the same order of magnitude as the detection. These phenomena may induce changes in the apparent spectrum related to the ranging aspects of the signal.

ACKNOWLEDGMENT

We should like to thank P. Gentien, former head of the Laboratory DEL/EC/PP at IFREMER, for the analysis of the water samples to be compared to the tank measurements. We also thank the European Commission who supported the research with a grant for Uwe Stute in the frame of the TMR program (Ref. ERBFMBICT 960629).

REFERENCES

1. Babichenko, S. and Poryvkina, L. 1997. Applications of tuneable LIDARs of FLS-Series in marine investigations. Proc. 3rd EARSeL Workshop on LIDAR Remote Sensing of Land and Sea, p. 60-65
2. Barbini, R., Colao, F., Fantoni, R., Palucci, A. and Ribezzo S. 1997. The ENEA mobile LIDAR fluorosensor equipment for marine campaigns. Proc. 3rd EARSeL Workshop on LIDAR Remote Sensing of Land and Sea, p. 15-22
3. Beeler SooHoo, J., Kiefer, D.A., Collins, D.J., McDermid, I.S. 1986. In-vivo fluorescence excitation and absorption apectra of marine phytoplankton: I. Taxonomic characteristics and responses to photoadaption. Journal of Plankton Research, p. 197-214
4. Chekalyuk, A. M., Demidov, A. A., Fadeev, V.V., Gorbunov, M.Yu. 1995. LIDAR Monitoring of phytoplankton and organic matter in the inner seas of Europe. EARSeL Advances in Remote Sensing, p. 131-139
5. Fadeev, V.V., Rubin, G.L. and Uvenkov, Ya.V. 1997. Remote laser diagnostics of photosynthetic organisms by the method of fluorescence saturation spectroscopy. Proc. 3rd EARSeL Workshop on LIDAR Remote Sensing of Land and Sea, p. 133-139
6. Harsdorf, S., Jannssen, M., Reuter, R. and Wachowicz, B. 1997. Submarine fluorescence LIDAR for environmental monitoring. Proc. 3rd EARSeL Workshop on LIDAR Remote Sensing of Land and Sea, p. 150-156

7. Hoge, F.E. and Swift, R.N. 1981. Airborne simultaneous spectroscopic detection of laser-induced water Raman backscatter and fluorescence from chlorophyll-a and other naturally occuring pigments. Applied Optics, 20(18), p. 3197-3205
8. Hofstraat, J.W., de Vreeze, M.E.J., van Zeijil, W.J.M., Peperzak, L., Peeters, J.C.H. and Balfort, H.W. 1991. Flow cytometric discrimination of phytoplankton classes by fluorescence emission and excitation properties. Journal of Fluorescence, 1(4), p: 249-265
9. Maffione, R.A. and Dana, D.R. 1997. Instruments and methods for measuring the backward-scattering coefficient of ocean waters. Applied Optics, 36(24), p. 6057-6067
10. Measures, R.M. 1984. Laser Remote Sensing. (Wiley, New York)
11. Ohm, K., Reuter, R., Stolze, M. and Willkomm R. 1997. Shipboard oceanographic fluorescence LIDAR development and evaluation based on measurements in the Antarctic waters. Proc. 3rd EARSeL workshop on LIDAR remote sensing of land and sea, p. 75-83
12. Pandithurai, G., Devara, P.C.S., Raj, P.E. and Sharma, S. 1996. Aerosol size distribution and refractive index from bistatic LIDAR angular scattering measurements in the surface layer. Remote Sens. Environ., p. 87-96
13. Reuter, R., Wang, H., Willkomm, R., Loquay, K., Hengstermann, T. and Braun: A laser fluorosensor for maritime surveillance: measurements of oil spills. EARSeL advances in Remote Sensing, 3(3), p. p. 152-169
14. Saito, T., Iitaka, H. and Sato, S. 1998. Measurements of phytoplankton distribution by an oceanographic compact LIDAR system for buoy observation. Ocean Optics XIV
15. Wang, H., Hengstermann, T., Reuter R. and Willkomm, R. 1992. Robust improvement in the signal-to-noise of a laser fluorosensor through selectively averaging signals. Rev. Sci. Instrum. 63, p. 1877-1897